Nanoarchitectonics
http://ojs.wiserpub.com/index.php/NAT/

Research Article

Synthesis of Metal Nanoparticles Encapsulated with Skewered Porphyrins Assembled by Siloxane Coupling

Olajumoke H. Olubowale[1], Quynh Do[1], Xochitl Gonzalez[1], Deja Hebert[1], Neepa Kurruppu Arachchige[1], Vladimir L. Kolesnichenko[2], Jayne C. Garno[1*]

[1]Chemistry Department, Louisiana State University, Baton Rouge, LA 70803, USA
[2]Chemistry Department, Xavier University, New Orleans, LA 70125, USA
E-mail: jgarno@lsu.edu

Received: 16 December 2023; **Revised:** 26 July 2022; **Accepted:** 27 July 2022

Abstract: A protocol for encapsulation of metal nanoparticles with organic shells of porphyrin molecules via silane coupling is described. A strategy with silicon tetrachloride was used to produce a skewered arrangement of porphyrins that are linked through a central silicon atom by siloxane, Si-O-Si bridges. The planar macrocycles align cofacially to surround the periphery of metal nanoparticles (e.g., gold and iron oxide). Skewered 'shish kebob' assemblies of porphyrins form an encapsulating shell by attachment to metal cores with silicon-oxygen-metal bridges. Free-base porphyrins were skewered through siloxane coupling using $SiCl_4$, with the silicon atom inserted into the center of the macrocycles. The Si atom binds to the four nitrogens at the center of the macrocycles and also links to adjacent macrocycles through siloxane bridges. Iron and gold nanoparticles were used as core materials, while the organic shells were prepared with tetraphenylporphyrin or octaethylporphyrin. The thickness of the shells can be tuned by synthetic parameters such as concentration and immersion intervals. Structural changes were tracked using ultraviolet–visible spectroscopy (UV/Vis) spectroscopy to evaluate spectral shifts. Nanoparticle samples were examined with tapping-mode atomic force microscopy to directly view changes in the size and shapes of nanoparticles before and after encapsulation with porphyrins. Phase images enabled sensitive mapping of the nanoparticle composition, revealing a soft organic shell surrounding the hard metal core. The synthetic approach with skewering porphyrins to metal nanoparticles should be generic for preparing metal core-shell nanoparticles encapsulated with shells of macrocyclic porphyrinoid molecules.

Keywords: core-shell nanoparticles, atomic force microscopy, silicon tetrachloride, silane coupling, porphyrins, tetraphenylporphyrin, octaethylporphyrin, metal-porphyrin nanoparticles

Nomenclature

TPP	Tetraphenylporphyrin
OEP	Octaethylporphyrin

DOI: https://doi.org/10.37256/nat.4220233446

1. Introduction

Multifunctional nanoparticles composed of hybrid materials such as organic coatings with an inorganic/metal core have been investigated because of the unique properties that can be tailored for specific applications. Diverse organic, polymeric, or biological moieties can be incorporated for the composition of organic coatings of nanoparticles to impart multiple functionalities, such as fluorescent, biomimetic, or therapeutic functions [1-3]. Practical applications with multifunctional nanoparticles have emerged for use in biomedical imaging [4-6], sensors [7, 8], drug delivery [9, 10], photodynamic therapy [11, 12], and catalysis [13]. The size and composition of metal nanoparticles can be precisely controlled to provide desirable properties such as conductivity, plasmon resonance, photon scattering, as well as magnetic or superparamagnetic properties. Gold nanoparticles have been used by artists centuries ago for their unique optical properties and fluorescence quenching capabilities [14]. Iron nanoparticles have useful magnetic properties, and surface modification can result in superparamagnetic iron oxide nanoparticles (SPION) which are used for magnetic imaging [15-17]. Functional groups can be added to metal nanoparticles by encapsulating the surface with selected molecules such as alkanethiols [18, 19], phosphines [20], fullerenes [21], cyclodextrins [22], dendrimers [23-25], and nucleic acids [26]. In this report, the interesting optical and electrical properties of porphyrins will be used to impart useful properties to encapsulated metal cores of gold or iron nanoparticles.

Several innovative strategies for preparing nanoparticles with porphyrins and phthalocyanines have been reported. Porphyrins are heterocyclic compounds that have four pyrrole rings and a five-membered structure linked by methine groups. Porphyrins can spontaneously self-assemble to form aggregate nanoparticles because of the π-conjugated system [27-40]. Aggregate assemblies formed with porphyrins are directed by π-π interactions, hydrogen bonding, noncovalent ionic bonds, metal-ligand bonds, van der Waals, and other specific intermolecular interactions [41-45]. The rigid aromatic architecture, thermal, and optical stability of porphyrinoids are promising for emerging developments in molecular electronics [46-48]. There are current applications with porphyrinoids for light harvesting [49, 50], catalysis [51-53], photonics [54, 55], sensors [56, 57], and photodynamic therapy [58]. Incorporating porphyrins into nanoparticles or surface assemblies can impart interesting optical, electronic, and multiple functionalities to nanoparticles [59-61].

Among the synthetic strategies that have been reported for preparing porphyrin nanoparticles, one approach is the ‘core-shell’ method of synthesizing nanoparticles of porphyrins. Core-shell nanoparticles are fabricated with an inner “core” nanoparticle and an outer “shell” such as with an organic film. The thickness and composition of the shell can be designed to introduce certain functionalities, such as photonic, electronic, adhesive, or biocompatibility [62, 63]. The size and composition of the core nanoparticle will likewise influence properties, such as electron transport and magnetic susceptibility. In the basic core-shell framework, materials such as metals, nanoparticles, silica, polymers, and porphyrinoids can be used as either the core or shell. Nanoparticles composed of a porphyrins as the “core” were surrounded by a shell of silica were prepared by Wang et al. [61]. The nanoparticles were synthesized with a sol-gel process and surfactant assisted self-assembly with zinc tetraphenylporphyrin (ZnTPP) and silicate precursors.

In recent reports, complex core-shell systems have been investigated by ab initio calculations. Improvements in computational resources have increased the simulation speed, accuracy, and accessibility and have become an essential research tool for understanding chemistry at the atomic/molecular level. Core-shell systems of inorganic nanomaterials have been studied with theoretical modeling to evaluate structural, dynamic and electronic properties. For example, self-induced InA1N core-shell nanorods synthesized by reactive magnetron sputter epitaxy (MSE) were studied using density functional theory (DFT) [64]. The thermal stability, elastic, and fracture resistant properties of 2D InBi (Indium Bismide) were studied with ab initio molecular dynamics (AIMD) simulations [65]. Information of nucleation and intercalation mechanisms that occur at the atomic scale were obtained through studies with density-functional molecular dynamics simulations of the reaction pathways responsible for the dissociation of the trimethylindium precursors with graphene [66].

We have developed a protocol to encapsulate metal nanoparticles with a porphyrin shell with an approach that is based on silicon coupling. In previous reports, nanostructures of silicon complexes of porphyrins and phthalocyanines were successfully prepared to form covalently bound structures on surfaces of silicon, glass, and indium tin oxide [67-69]. The orientation of porphyrins on surfaces is determined by factors such as the nature of the peripheral substituents and their position on the macrocycle. The strategy of preparing a coplanar, skewered arrangement of OEP multilayers that are mediated by covalent Si-O bonds has been previously described [70]. Herein, we present results for linking

porphyrins with Si-O-Si bridges to metal nanoparticles. A silane coupling mechanism was applied to prepare core-shell nanoparticles encapsulated with porphyrins for metal cores of gold and iron. The free-base porphyrins selected were 2,3,7,8,12,13,17,18-octaethylporphyrin, and 5,10,15,20-tetraphenyl-21H,23H-porphine. Parameters such as the concentration, solvent nature and immersion intervals were systematically evaluated for preparing samples of nanoparticles. Samples were characterized with tapping-mode atomic force microscopy (AFM) and with ultraviolet–visible spectroscopy (UV/Vis) spectroscopy.

2. Materials and methods

2.1 *Materials and reagents*

Silicon tetrachloride and 2,3,7,8,12,13,17,18-octaethylporphyrin were obtained from TCI America (Portland, OR); and 5,10,15,20-tetraphenyl-21H,23H-porphine was obtained from Sigma-Aldrich (St. Louis, MO). Either freshly cleaved ruby muscovite mica (S&J and Trading Co., NY) or glass coverslips, 12 mm diameter (VWR, Radnor, PA) were used as substrates. Piranha solution was prepared with sulfuric acid (98.0%) (J. T. Baker, Fisher Scientific) and a solution of 30% hydrogen peroxide (VWR) for cleaning the glass substrates. Glass substrates were then rinsed with ethanol, dried in air, and irradiated with ozone (50 min). Absolute ethanol was obtained from Deacon Labs (Prussia, PA). Milli-Q type 1 water, (18 megohm, Millipore, Bedford, MA) was used for rinsing steps. Chloroform (HPLC grade) was acquired from Fisher Scientific (Lenexa, KS), and toluene from EMD Millipore Corporation (Billerica, MA). Gold (III) chloride trihydrate and trisodium citrate were both obtained from Sigma-Aldrich (St. Louis, MO).

2.2 *Synthesis of metal nanoparticles*

Superparamagnetic Fe_2O_3 nanoparticles were synthesized as previously reported [71, 72]. Maghemite (g-Fe_2O_3) nanoparticles were synthesized as a surfactant-free non-aqueous (diethylene glycol) colloid. Synthesis was accomplished by high-temperature hydrolysis of chelated iron(II,III) alkoxide complexes, followed by oxygenation at room temperature. Gold nanoparticles were prepared using the citrate-reduction protocol as published previously [73]. A solution (125 mL) of 0.25 mM gold (III) chloride trihydrate was boiled under reflux at 300 °C in a round bottom flask. An aliquot of 6.25 mL of 40 mM trisodium citrate was then added to the heated gold solution under reflux. Within 10 min, the solution transformed from clear to a rose-pink color. The solution was removed from heat and stirred at room temperature for 30 min.

2.3 *Encapsulation of iron oxide nanoparticles with silane-coupled tetraphenylporphyrins (Si-TPP)*

A solution of 0.5 mM TPP (5 mL) was mixed with 5 µL silicon tetrachloride and stirred at room temperature for 8 min. After stirring, 1 mL of a diluted solution of Fe_3O_4 nanoparticles was added. The solution was then stirred for 24 h.

2.4 *Encapsulation of gold nanoparticles with silane-coupled octaethylporphyrin (Si-OEP)*

A solution of 0.5 mM OEP (5 mL) was mixed with 5 µL of silicon tetrachloride in chloroform. The mixture was stirred for 5 min, followed by the addition of 1 mL of the gold nanoparticle solution. Stirring was continued for 24 h.

2.5 *AFM*

A model 5420 atomic force microscope from Agilent Technologies (Santa Clara, CA) was used to characterize samples. Silicon probes with an aluminum reflex coating were used to acquire images in tapping mode; either model Tap300Al-G probes with a resonance frequency of 300 kHz and a force constant of 40 N/m (BudgetSensors, Bulgaria) or SCOUT 350 RAl tips with a resonance frequency of 350 kHz and a spring constant of 42 N/m (NuNano, Bristol, UK) were used for AFM studies. Gwyddion software (Version 2.52) was used for analysis and digital processing of AFM images [74].

2.6 *UV/Vis spectroscopy*

A Cary 50 Bio UV/Vis spectrophotometer was used for acquiring absorbance spectra of solutions of nanoparticles and porphyrins for solutions within quartz cuvettes.

3. Results

3.1 *Encapsulation of metal nanoparticles with siloxane-linked porphyrins*

The protocol for preparing metal nanoparticles encapsulated with porphyrins using silane coupling is depicted in Figure 1. When silicon tetrachloride is added to a solution of porphyrins, a silicon atom is inserted into the center of the porphyrin macrocycles. The four nitrogen atoms of the conjugated porphyrin macrocycle bind tightly to the central silicon atom with two chlorides connected at opposite faces of the macrocycles that facilitate hydrolysis self-assembly reactions for binding assemblies to the nanoparticle as well as to form covalent Si-O bonds to adjacent molecules.

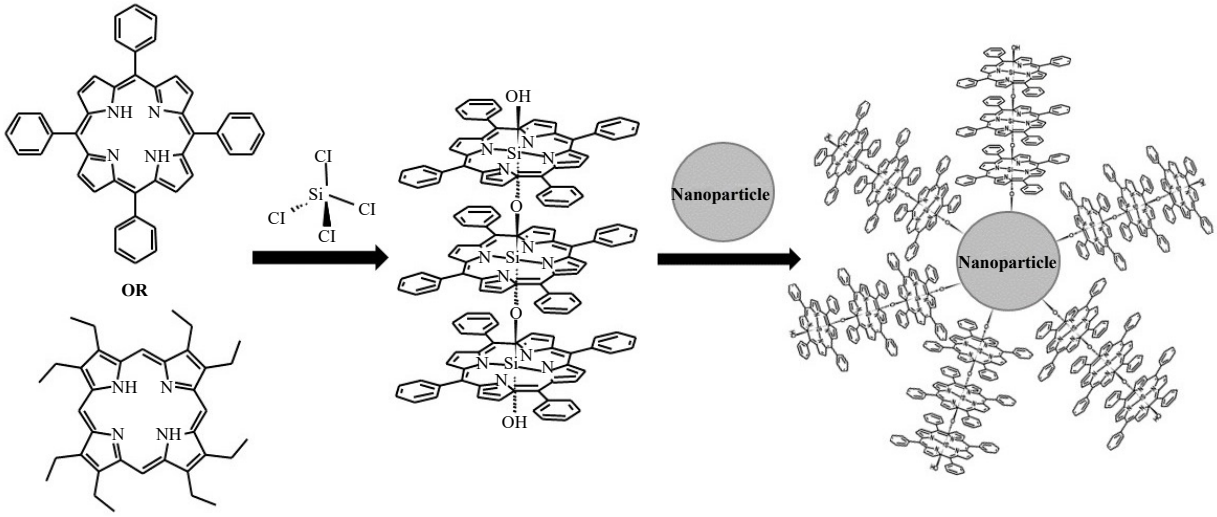

Figure 1. Skewered arrangement of porphyrins linked covalently to metal nanoparticles by silane coupling and self-assembly

To prepare porphyrin-encapsulated core-shell nanoparticles, a precursor solution was prepared by mixing the free-base porphyrin and $SiCl_4$. An aliquot of metal nanoparticles was added to the mixture to attach porphyrins through siloxane self-assembly. A "shish kebob" arrangement of cofacially aligned porphyrins is formed with siloxane, Si-O-Si bridges between macrocycles. Porphyrins bind to adjacent molecules aligned in a cofacial arrangement linked through the centers of the macrocycles. Each of the central silicon groups coordinated within the porphyrin macrocycles becomes hydrolyzed for linking either to adjacent molecules or to metal nanoparticles. The hydroxyl groups bind through self-assembly steps of hydrolysis and condensation to generate core-shell metal nanoparticles that are encapsulated with porphyrins in a skewered configuration. The molecules form an organic shell surrounding the metal nanoparticles, in which the macrocycles are oriented in a stacked, coplanar fashion, following the curved geometry of the central core nanoparticle.

Previous studies have reported that the planar macrocycles are oriented in a cofacial arrangement to form multilayer films on flat substrates [70, 75]. The assembly process to generate porphyrin multilayers was monitored with UV/Vis spectroscopy and the bond length between the stacked aromatic ring was investigated with X-ray diffraction studies, as reported by Lee et al. [75]. Using tetraphenylporphyrinatosilicon(IV) chloride as a building block, the molecules were shown to assemble in a layer-by-layer process to generate a cofacial arrangement within the multilayer films for samples that were prepared with ITO or glass substrates.

3.2 *Tapping-mode AFM characterization of uncoated iron oxide (Fe_3O_4) nanoparticles*

Dilute solutions of magnetite nanoparticle were deposited on glass and mica substrates to obtain AFM images of the uncoated nanoparticles. The surface coverage was tuned by successive dilutions (1,000-100,000-fold) to obtain sparse surface coverage so that the 3D shapes of the nanoparticles could be resolved. An aliquot of 20 µL of a nanoparticle solution was dried on freshly cleaved mica and dried in ambient air for the images presented in Figure 2. Mica substrates are commonly used for AFM sample preparation because it is atomically flat with a net negative charge for electrostatic attachment of nanomaterials. The hydrophilic nature of mica has advantages for minimizing aggregation of nanoparticles. Topography and phase images reveal a random arrangement of relatively monodisperse nanoparticles with a spherical shape. An example height profile discloses a height of approximately 7 nm (Figure 2C) for three nanoparticles, referencing uncovered areas of the substrate as a baseline. Analysis of several images indicates that overall, the Fe_3O_4 nanoparticles range in size from 0.4 to 15 nm, with an average diameter measurement of 4.2 ± 0.3 nm (n = 98).

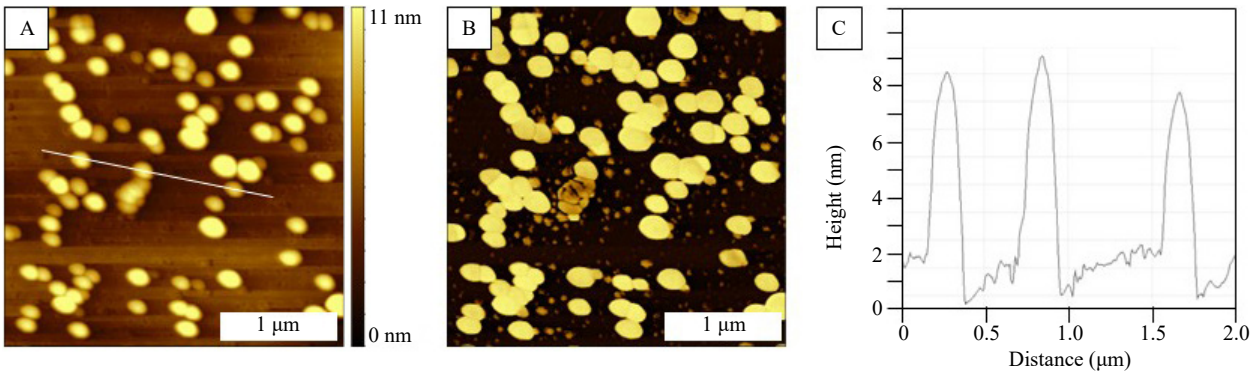

Figure 2. Iron oxide nanoparticles prepared on freshly cleaved mica substrates. A - topography image (3 × 3 µm^2); B - corresponding phase image; C - cursor profile for the white line drawn in A. Images were acquired with tapping-mode AFM

A strategy for sample preparation by immersion was tested with glass slides that were rendered hydrophilic by acid cleaning and ozone treatment, shown in Figure 3. Cleaned glass substrates were immersed in a solution of Fe_3O_4 nanoparticles for 24 min and then dried in air. Well-dispersed, spherical iron oxide nanoparticles are visible in the topography frame (Figure 3A). The differences in contrast for the hard metal cores and softer organic shells are sensitively-distinguished in the simultaneously acquired phase image of Figure 3B. In phase frames, the dark dots pinpoint the central metal core of the nanoparticles. Each nanoparticle is surrounded with a bright halo which indicates the soft organic shell of a physisorbed surfactant film. A representative height profile drawn across two nanoparticles indicates a height of ~5 nm (Figure 3C).

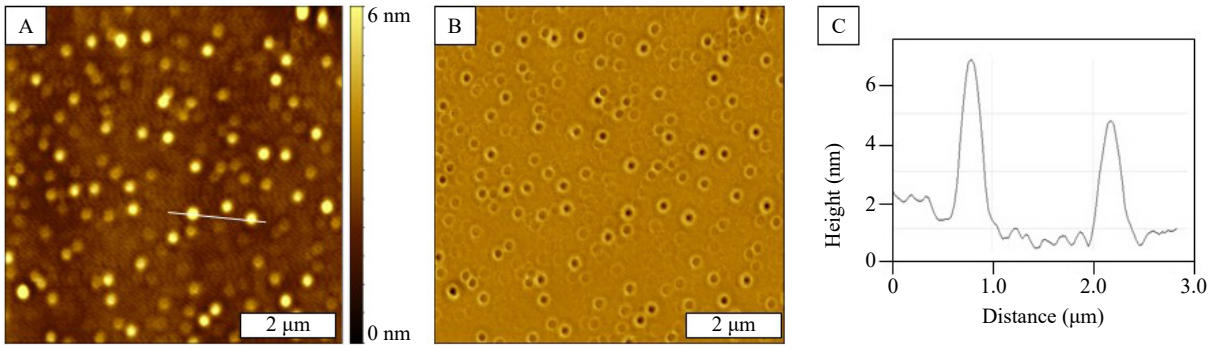

Figure 3. Iron oxide nanoparticles prepared on glass by an immersion protocol. A - topography image (8 × 8 µm^2); B - corresponding phase image; C - cursor profile for the white line in A

The nanoparticles resolved within the topography frames are well-dispersed with relatively uniform spherical geometries. The halos were not detected for the sample prepared with mica substrates because it can be difficult to find the optimum driving frequency for sensitive detection of the surfactant coating when using tapping mode. Interestingly, the contrast differences for the core-shell chemistry were readily detected when samples were prepared on glass substrates, as revealed in Figure 3. This observation suggests that the hard surface of glass has influenced the hard/soft interactions of the tapping AFM probe for detecting changes in phase response.

3.3 *Characterization of Si-TPP encapsulated iron oxide nanoparticles*

Core-shell nanoparticles were synthesized by adding solutions of metal nanoparticles to a mixture of porphyrin and $SiCl_4$, as previously described in Sections 2.3 and 2.4. Parameters of concentration and duration of stirring can be designed to tune the thickness of the organic shell. Core-shell nanoparticles prepared with Fe_3O_4 nanoparticles (magnetite) were prepared with TPP on a glass substrate, shown in Figure 4. A random arrangement of ~20 nanoparticles encapsulated with Si-TPP are observed in the topography frame of Figure 4A. The bright halo surrounding each of the nanoparticles in the corresponding phase image pinpoints the differences in elastic response between the core of the Fe_3O_4 nanoparticles and the surrounding soft porphyrin coating (Figure 4B). The bright halo observed in Figure 4B could possibly be attributable to edge effects from AFM imaging, or to residual surfactants not fully displaced by the siloxane-linked porphyrins. However, there is clear evidence that multilayers of porphyrins have been attached to the iron oxide nanoparticles revealed by UV/Vis studies, which demonstrate spectral shifts before and after reaction with $SiCl_4$. The height of the Si-TPP nanoparticles measured ~ 7 nm (Figure 4C). Further analysis of the sizes for core-shell Fe_3O_4 nanoparticles with Si-TPP from this experiment revealed an average diameter of 6.3 ± 1.4 nm (n = 21), confirming that adding an organic shell of TPP increased the overall size of the nanoparticles.

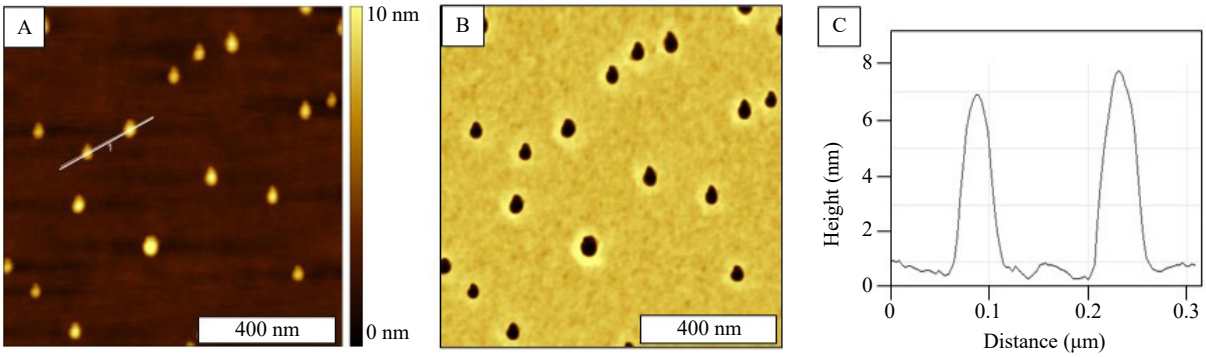

Figure 4. Iron oxide nanoparticles encapsulated with Si-TPP. The sample was prepared on a glass slide by drop deposition. A - topographic image (1 × 1 µm^2); B - concurrently acquired phase image; C - height profile for the line in A

The parameters of concentration and varying the duration of substrate immersion were evaluated for tailoring the thickness of the encapsulating porphyrin shell. Glass substrates were immersed in core-shell nanoparticles for samples prepared with selected parameters of immersion time and concentrations. After the substrate was immersed for 7 min the sample exhibits nearly spherical nanoparticles without surface aggregation for the topography frames of Figures 5A and 5D. The phase images do not clearly distinguish between the outer coating and central metal core (Figures 5B and 5E). Cursor profiles across several nanoparticles reveal heights which measure 4-7 nm. Based on the size analysis of the uncoated particles, the size is 2.4 ± 0.9 nm, after coating with the porphyrin, the size increased to 4.0 ± 1.2 nm (Figure 5), indicating an increase in the thickness of the organic shell. Evidence of coordination of silicon tetrachloride to the center of the free base porphyrin and encapsulation is apparent with spectral shifts detected by UV/Vis spectroscopy (Figure 6). Visible color changes were observed during the reaction of Fe_3O_4 nanoparticles with silicon tetrachloride-tetraphenylporphyrin. The pink color of the TPP in toluene changed to green after the addition of $SiCl_4$. The spectral shift from 420 to 450 nm reflects changes when the macrocycle expanded to make room to accommodate a silicon atom at the center of the ring. After adding the Fe_3O_4 nanoparticles, the color of the solution turned deep green, and there are

two bands that are observed: a prominent intense band at 420 nm and a weaker band from 450 nm. Typically, porphyrins have a characteristic Soret band (strong transition to the second excited state) at shorter wavelengths around 400 nm and Q bands (weak transitions/absorptions) at longer wavelengths from 500 to 700 nm. However, with variations in appended substituents or the insertion of elements within the macrocycle, the absorption spectrum changes accordingly. The UV/Vis spectra show the Soret band of TPP at ~415 nm, and there are four broad Q bands. After coordination with $SiCl_4$, a broad Soret band and two characteristic Q bands were observed, which can be attributed to the insertion of Si into the center of the free base porphyrin. After encapsulating Fe_3O_4 nanoparticles with Si-TPP, an intense Soret band with four characteristic Q bands becomes apparent.

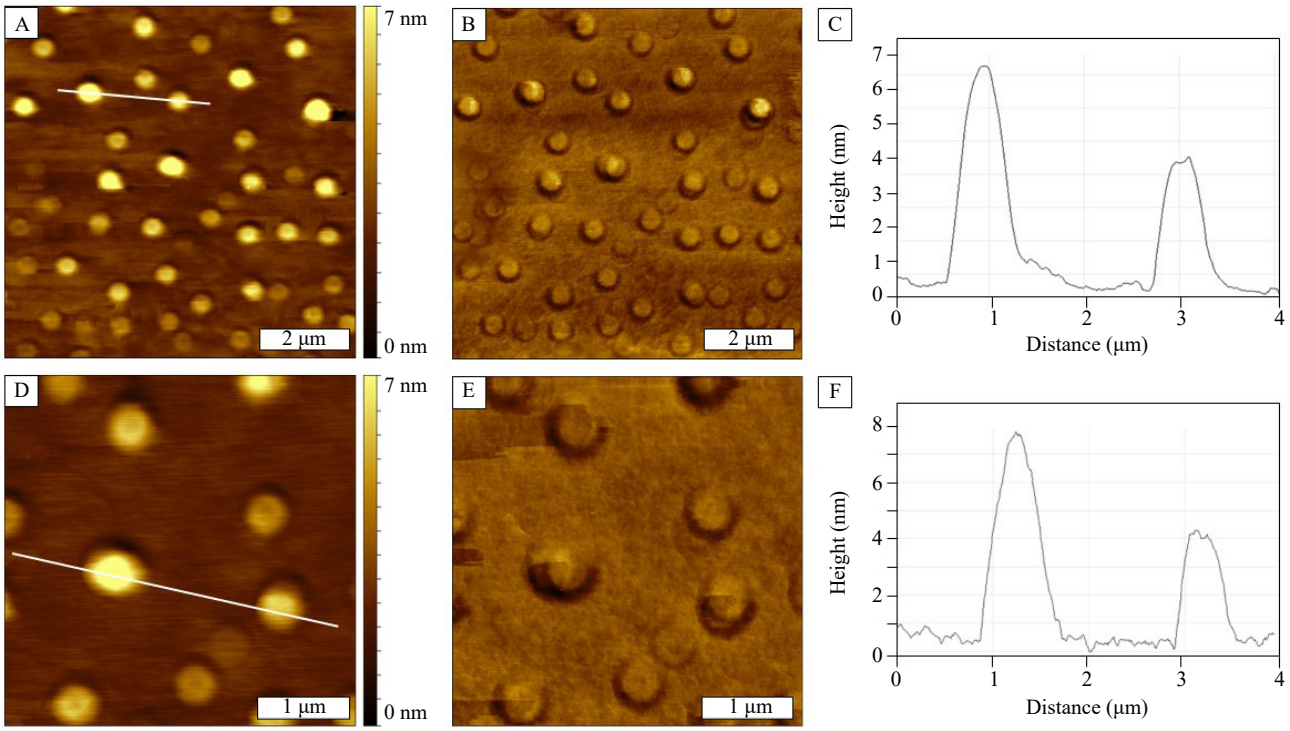

Figure 5. Iron oxide nanoparticles encapsulated with Si-TPP. A - topography frame (8 × 8 µm^2); B - corresponding phase image; C - height profile for the line in A; D - higher magnification topograph (4 × 4 µm^2); E - matching phase frame; F - height profile for the line in D

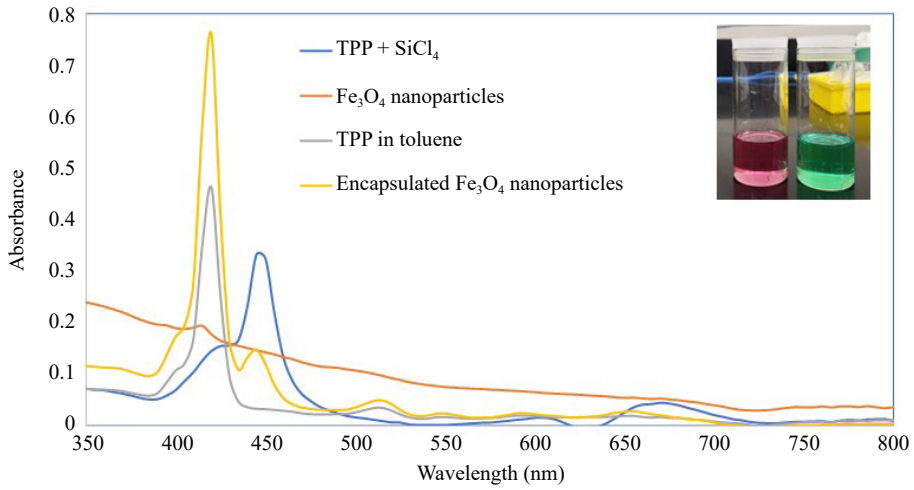

Figure 6. Characterization of nanoparticle samples with UV/Vis spectroscopy. The inset photograph shows the change in color from pink to green when $SiCl_4$ was added to a TPP solution in toluene

3.4 *AFM Characterization of Si-OEP encapsulated Fe_3O_4 nanoparticles*

The applicability of the synthetic approach for skewering porphyrin assemblies to Fe_3O_4 nanoparticles was tested with OEP. Glass substrates were immersed in the nanoparticle solutions for 8 min, dried, and then imaged in ambient air with AFM. The topography frames (Figure 7) reveal nanoparticles with regular spherical shapes dispersed throughout the framed areas. Interestingly, the phase images disclose contrast differences for sample softness, with dark spots indicating the encapsulated metal cores in the center of each nanoparticle. The heights of the nanoparticles measured 2-4 nm, shown with example cursor profiles (Figures 7C and 7F).

3.5 *Encapsulation of gold nanoparticles with Si-OEP*

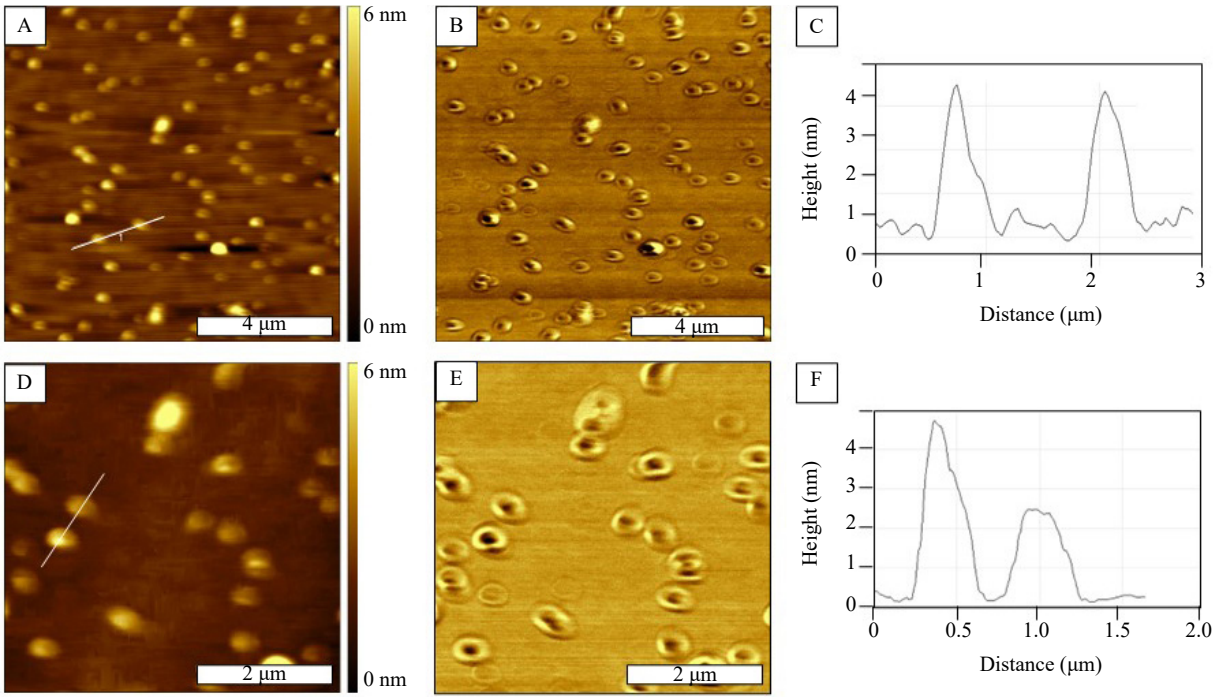

Figure 7. Core-shell Fe_3O_4 nanoparticles prepared with Si-OEP prepared on a glass slide by immersion. A - topographic image (10 × 10 µm^2); B - simultaneously acquired phase frame; C - height profile for the line in A; D - higher magnification topograph (5 × 5 µm^2); E - phase image for C; F - height profile for the line in D

The strategy for skewering porphyring assemblies to nanoparticles was tested with a different metal material by using gold cores. Encapsulation of gold nanoparticles with OEP was accomplished as presented in Figure 8. A solution of uncoated gold nanoparticles was dried on glass substrates and compared to samples prepared with Si-OEP encapsulated core-shell nanoparticles. A close-up view of the uncoated gold nanoparticles are shown with topography and phase images in Figures 8A and 8B, respectively. The height measured ~2 nm, shown with an example cursor profile in Figure 8C. After encapsulation of the gold nanoparticles with a Si-OEP shell, surface views exhibit randomly dispersed nanoparticles (Figure 8D and 8E). The heights are slightly larger, an example cursor profile is displayed in Figure 8F for three nanoparticles measuring 2.8, 2.3, and 2.6 nm. A bright halo is observed to surround the dark central gold core of each nanoparticle, indicating that a soft organic film encapsulates each Au nanoparticle.

Encapsulation was successful as evidenced by height measurements and phase images. The height of the gold nanoparticles increased after coating with Si-OEP, indicating a change of nanoparticle size due to the addition of a coating of porphyrin. The analysis of height profiles for multiple samples and images, an average height of 2.4 ± 0.3 nm (n = 50) was measured for bare Au nanoparticles, and the diameter increased for the Si-OEP encapsulated Au nanoparticles which measured 7.7 ± 0.2 nm (n = 50). In the phase images, the bright halo indicates the presence of a soft

porphyrin shell around a nanoparticle. This shows that a multilayer coating has formed which has sufficient thickness to be detectable with a tapping AFM probe, and confirms that the increase in nanoparticle size is due to the attachment of Si-OEP.

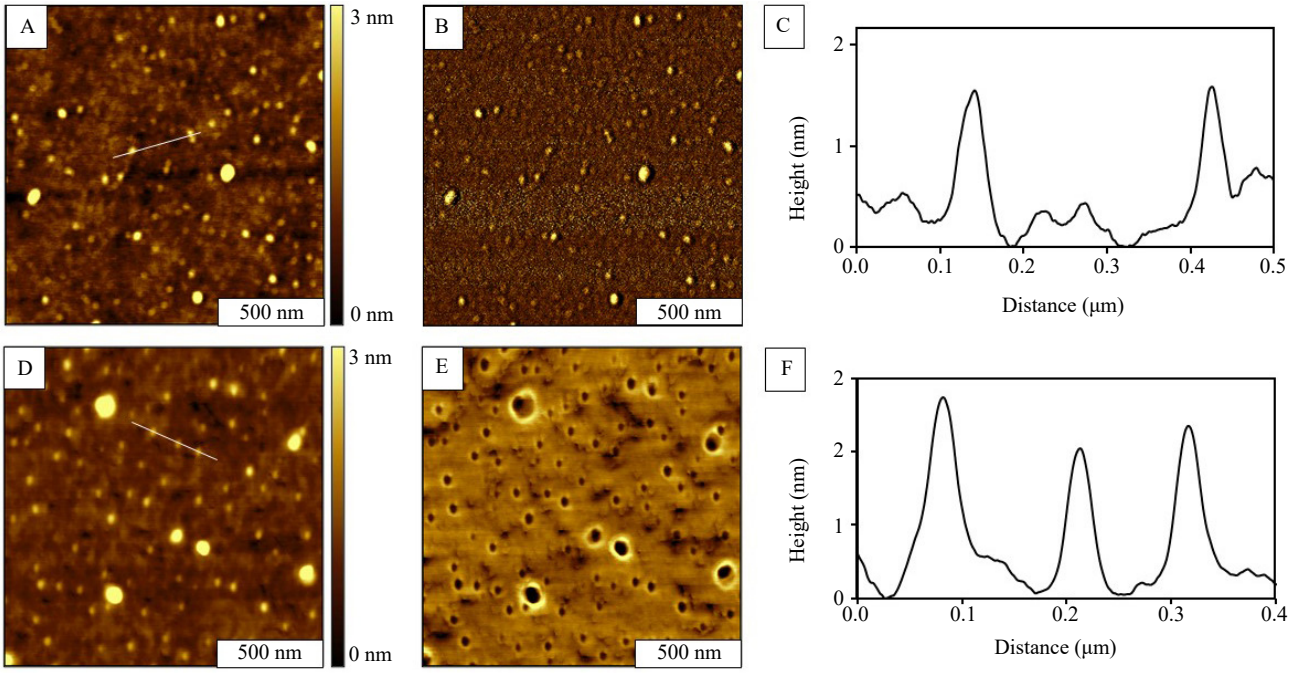

Figure 8. Encapsulation of gold nanoparticles with OEP. A - topography; B - phase images of uncoated gold nanoparticles. C - height profile for the line drawn in A; D - topography; E - phase images of encapsulated gold nanoparticles; F - height profile of the line drawn in D. Samples were prepared on glass substrates, 2 × 2 μm^2 AFM views

Visible color changes were observed for each reaction mixture during the preparation of Au nanoparticles encapsulated with Si-OEP, which is attributable to chemical changes for each step. Photos of the colorful solutions at each step are shown in Figures 9A-E. A change in color is visible between subsequent solutions, from pink to magenta as $SiCl_4$ is added to the OEP solution and to dark violet as the pale pink nanoparticle solution is added. Absorbance spectra of each solution were also obtained, with the solutions diluted as necessary to optimize absorbance values (Figure 8F). The characteristic Soret band at 400 nm and Q bands in the 500-600 nm region are observed for the solutions containing OEP.

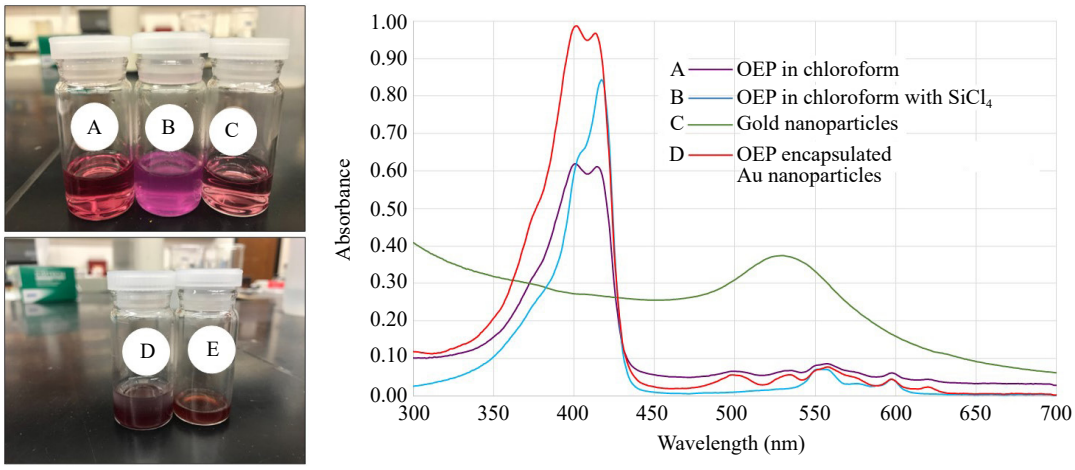

Figure 9. Characterization of OEP encapsulated gold nanoparticles by UV/Vis spectroscopy. (Left) Photographs depicting solutions: A - OEP in chloroform; B - the OEP-chloroform solution after addition of $SiCl_4$; C - solution of gold nanoparticles; D - solution of gold nanoparticles encapsulated with OEP; E - diluted solution of OEP-Au nanoparticles. (Right) Absorbance spectra of each solution

A peak shift for the Soret and Q bands was observed after addition of $SiCl_4$ to the reaction vessel, where the blue spectral line representing Si-OEP is red-shifted compared to the purple line of OEP in chloroform (Figure 9). The color changes in each solution are attributable to the effects of changes in the macrocycle geometry of OEP when Si is inserted within the macrocycles and also when the molecules attach to gold nanoparticles. Analysis of the green spectral line shows a broad peak for the Au nanoparticles in the range of 520 and 580 nm, consistent with previously published spectra of gold nanoparticle solutions. After the addition of gold nanoparticles to the solution of Si-OEP, the peak associated with gold nanoparticles is no longer present at around 540 nm, and the absorbance spectrum appears similar to a solution of Si-OEP, as shown by the red spectral line. The absorption peaks of the iron and gold nanoparticles do not significantly contribute to the spectrum of the final encapsulated nanoparticle.

With UV/Vis absorption, changes to the shape of the free-base porphyrins can be tracked. Evidence that Si was successfully coordinated to the macrocycles of OEP can be readily detected by observing shifts in the Soret and Q bands using UV/Vis spectroscopy. Structural changes of the central atom or pendant substituents on the ring will also affect the transition energies profiled in absorbance spectra. The absorption bands in systems of chromophoric porphyrins arise from electronic transitions between the two HOMOs and LUMOs of the aromatic rings of the macrocycle, indicating pi-pi transitions [76]. When $SiCl_4$ is added to a solution of OEP, there is a characteristic red shift for the broad Soret band centered around 400 nm, which can be attributed to changes in molecular geometry when a Si atom is incorporated within the macrocycle. Differences in spectra for the Q bands were also detected, exhibiting a characteristic red shift (purple vs. red spectral lines in Figure 9).

4. Discussion

Comparing the sizes of the nanoparticles before and after encapsulation gives us an indication of the thickness of the organic shells. Measurements of height obtained from AFM images were used to estimate the diameter of nanoparticles, and are summarized in Table 1. The extent of polydispersity at the nanoscale is indicated by the error terms (standard error values). For the Si-TPP nanoparticles prepared with Fe_3O_4 cores (Figures 4 and 5), the diameter increased by 4.5 and 1.6 nm, respectively, with the addition of an organic shell. For the Si-OEP nanoparticles prepared with Fe_3O_4 and Au cores (Figures 7 and 8D), the diameter increased by 1.0 and 5.3 nm, respectively. The height of a porphyrin molecule aligned in a coplanar orientation measures 0.4 nm; thus, the thickness of the coatings corresponds to approximately 11 molecules (Figure 4), 4 molecules (Figure 5), 2 molecules (Figure 7), and 16 molecules (Figure 8B). The measurements are based on the cofacial orientation of the macrocycles that were assembled in a skewered arrangement linked with Si-O-Si bridges. The change in diameter between the uncoated and coated nanoparticles is evidence that the porphyrin molecules were successfully attached to the metal nanoparticles. The differences in the

number of attached porphyrin molecules can be attributed to changes in the time intervals for the synthesis, since longer intervals produced thicker coatings. The core-shell nanoparticles in Figures 4 and 8D were mixed for at least 12 h after adding solutions of the metal nanoparticles. For the nanoparticles shown in Figures 5 and 7, the reaction took place for ~2-3 h. Further time-dependent studies will be designed to determine if porphyrin molecules spontaneously skewer upon reaction with silicon tetrachloride or if this takes place by assembly from the surface of the nanoparticles. A further critical factor for synthesis is the stoichiometry of $SiCl_4$ and porphyrin for controlling the shell thickness.

Table 1. Principles of sustainable and livable sidewalks [19]

Sample description	Size range (nm)	Diameter (nm)
Uncoated Fe_3O_4 nanoparticles (Figure 3)	0.5 - 5.3	2.4 ± 0.9 nm (n = 83)
TPP + Fe_3O_4 nanoparticles (Figure 4)	5.5 - 9.4	6.9 ± 0.9 nm (n = 17)
TPP + Fe_3O_4 nanoparticles (Figure 5)	3.0 - 6.7	4.0 ± 1.2 nm (n = 9)
OEP + Fe_3O_4 nanoparticles (Figure 7)	2.1 - 3.8	3.3 ± 1.0 nm (n = 10)
Uncoated Au nanoparticles (Figure 8A)	1.4 - 4.4	2.4 ± 0.3 (n = 50)
OEP + Au nanoparticles (Figure 8D)	3.8 - 9.8	7.7 ± 0.2 nm (n = 50)

A further direction for investigations with porphyrin core-shell nanoparticles will be to directly evaluate the long term stability of the nanoparticles. After intervals of several months, the suspensions will be characterized with UV/Vis and AFM studies to evaluate if the coatings persist, or if samples tend to aggregate over time. Since porphyrins are robust structures that do not degrade with heat or oxidation, the stability of nanoparticle solutions can be verified.

5. Conclusion

Silane coupling of porphyrins with silicon tetrachloride can be used to prepare metal core-shell nanoparticles with a covalently attached organic shell. Porphyrins were attached to Au and Fe_3O_4 nanoparticles using silane coupling to adapt a skewered configuration. Using simple mixing steps, silicon molecules were coordinated to the center of free-base porphyrins (TPP and OEP), which also connect to other macrocycles via Si-O-Si bridges. The assemblies were anchored to the surface of metal nanoparticles by covalent Si-O-metal bonds so that the planar porphyrin molecules were oriented cofacially in a skewered arrangement. Visual color changes and spectra from UV/Vis measurements confirm that encapsulated nanoparticles were synthesized. Tapping-mode phase images of core-shell nanoparticles sensitively reveal differences in contrast between the hard inner metal core and surrounding organic shells of porphyrin-encapsulated nanoparticles. Experiments using TPP and OEP with Au and Fe_3O_4 nanoparticles demonstrate that this technique can be generic for the synthesis of other core-shell nanoparticles with a metal core and an organic porphyrin shell. Future directions are to test if silane coupling can be used with free-base phthalocyanines, and the effects of porphyrin ligands on the conductive or optical properties of core-shell nanoparticles will be investigated.

Acknowledgments

We thank D. I. Senadheera for their helpful comments. The authors gratefully acknowledge financial support from the Louisiana Board of Regents Support Fund, Traditional Enhancement Program (LEQSF(2014-16)-ENH-TR-03).

Conflict of interest

There is no conflict of interest for this study.

References

[1] Sanvicens N, Marco MP. Multifunctional nanoparticles - properties and prospects for their use in human medicine. *Trends Biotechnology*. 2008; 26(8): 425-433. Available from: https://doi.org/10.1016/j.tibtech.2008.04.005.

[2] Liong M, Lu J, Kovochich M, Xia T, Ruehm SG, Nel AE, et al. Multifunctional inorganic nanoparticles for imaging, targeting, and drug delivery. *ACS Nano*. 2008; 2(5): 889-896. Available from: https://doi.org/10.1021/nn800072t.

[3] Jin Y, Jia C, Huang S-W, O'Donnell M, Gao X. Multifunctional nanoparticles as coupled contrast agents. *Nature Communications*. 2010; 1: 41. Available from: https://doi.org/10.1038/ncomms1042.

[4] Grigore ME, Ion R-M, Iancu L, Grigorescu RM. Tailored porphyrin–gold nanoparticles for biomedical applications. *Journal of Porphyrins and Phthalocyanines*. 2019; 23(7-8): 766-780. Available from: https://doi.org/10.1142/S108842461930012X.

[5] Huang H, Song W, Rieffel J, Lovell JF. Emerging applications of porphyrins in photomedicine. *Frontiers in Physics*. 2015; 3: 23. Available from: https://doi.org/10.3389/fphy.2015.00023.

[6] Wang J, Gao S, Wang X, Zhang H, Ren X, Liu J, et al. Self-assembled manganese phthalocyanine nanoparticles with enhanced peroxidase-like activity for anti-tumor therapy. *Nano Research*. 2022; 15: 2347-2354. Available from: https://doi.org/10.1007/s12274-021-3854-5.

[7] Liu Q, Chen P, Xu Z, Chen M, Ding Y, Yue K, et al. A facile strategy to prepare porphyrin functionalized ZnS nanoparticles and their peroxidase-like catalytic activity for colorimetric sensor of hydrogen peroxide and glucose. *Sensors and Actuators B: Chemical*. 2017; 251: 339-348. Available from: https://doi.org/10.1016/j.snb.2017.05.069.

[8] Sousa LM, Vilarinho LM, Ribeiro GH, Bogado AL, Dinelli LR. An electronic device based on gold nanoparticles and tetraruthenated porphyrin as an electrochemical sensor for catechol. *Royal Society Open Science*. 2017; 4(12): 170675. Available from: https://doi.org/10.1098/rsos.170675.

[9] Emerich DF, Thanos CG. The pinpoint promise of nanoparticle-based drug delivery and molecular diagnosis. *Biomolecular Engineering.* 2006; 23(4): 171-184. Available from: https://doi.org/10.1016/j.bioeng.2006.05.026.

[10] Allen TM, Cullis PR. Drug delivery systems: Entering the mainstream. *Science*. 2004; 303(5665): 1818-1822. Available from: https://doi.org/10.1126/science.1095833.

[11] Mondal D, Bera S. Porphyrins and phthalocyanines: Promising molecules for light-triggered antibacterial nanoparticles. *Advances in Natural Sciences: Nanoscience and Nanotechnology*. 2014; 5(3): 033002. Available from: https://doi.org/10.1088/2043-6262/5/3/033002.

[12] Wang Z, Gai S, Wang C, Yang G, Zhong C, Dai Y, et al. Self-assembled zinc phthalocyanine nanoparticles as excellent photothermal/photodynamic synergistic agent for antitumor treatment. *Chemical Engineering Journal*. 2019; 361: 117-128. Available from: https://doi.org/10.1016/j.cej.2018.12.007.

[13] Lokesh KS, Shambhulinga A, Manjunatha N, Imadadulla M, Hojamberdiev M. Porphyrin macrocycle-stabilized gold and silver nanoparticles and their application in catalysis of hydrogen peroxide. *Dyes and Pigments*. 2015; 120: 155-160. Available from: https://doi.org/10.1016/j.dyepig.2015.04.002.

[14] Talapin DV, Shevchenko EV. Introduction: Nanoparticle chemistry. *Chemical Reviews*. 2016; 116(18): 10343-10345. Available from: https://doi.org/10.1021/acs.chemrev.6b00566.

[15] Gupta AK, Gupta M. Synthesis and surface engineering of iron oxide nanoparticles for biomedical applications. *Biomaterials*. 2005; 26(18): 3995-4021. Available from: https://doi.org/10.1016/j.biomaterials.2004.10.012.

[16] Hao R, Xing R, Xu Z, Hou Y, Gao S, Sun S. Synthesis, functionalization, and biomedical applications of multifunctional magnetic nanoparticles. *Advanced Materials*. 2010; 22(25): 2729-2742. Available from: https://doi.org/10.1002/adma.201000260.

[17] Khurshid H, Hadjipanayis CG, Chen H, Li W, Mao H, Machaidze R, et al. Core/shell structured iron/iron-oxide nanoparticles as excellent MRI contrast enhancement agents. *Journal of Magnetism and Magnetic Materials*. 2013; 331: 17-20. Available from: https://doi.org/10.1016/j.jmmm.2012.10.049.

[18] Hu J, Zhang J, Liu F, Kittredge K, Whitesell JK, Fox MA. Competitive photochemical reactivity in a self-assembled monolayer on a colloidal gold cluster. *Journal of the American Chemical Society*. 2001; 123(7): 1464-1470. Available from: https://doi.org/10.1021/ja003180l.

[19] Takao O, Katsuhiro I, Satoko N, Kazushi M. Enhancement of self-assembly of large (>10 nm) gold nanoparticles on an ITO substrate. *Applied Physics Express.* 2014; 7(6): 065001. Available from: https://doi.org/10.7567/APEX.7.065001.

[20] Cano I, Huertos MA, Chapman AM, Buntkowsky G, Gutmann T, Groszewicz PB, et al. Air-stable gold nanoparticles ligated by secondary phosphine oxides as catalyst for the chemoselective hydrogenation of substituted aldehydes: A remarkable ligand effect. *Journal of the American Chemical Society*. 2015; 137(24): 7718-

7727. Available from: https://doi.org/10.1021/jacs.5b02802.
[21] Islam MT, Molugu SK, Cooke PH, Noveron JC. Fullerene stabilized gold nanoparticles. *New Journal of Chemistry*. 2015; 39(8): 5923-5926. Available from: https://doi.org/10.1039/C5NJ01367D.
[22] Zhao Y, Huang Y, Zhu H, Zhu Q, Xia Y. Three-in-one: Sensing, self-assembly, and cascade catalysis of cyclodextrin modified gold nanoparticles. *Journal of the American Chemical Society*. 2016; 138(51): 16645-16654. Available from: https://doi.org/10.1021/jacs.6b07590.
[23] Kainz QM, Reiser O. Polymer-and dendrimer-coated magnetic nanoparticles as versatile supports for catalysts, scavengers, and reagents. *Accounts of Chemical Research*. 2014; 47(2): 667-677. Available from: https://doi.org/10.1021/ar400236y.
[24] Scott RW, Wilson OM, Crooks RM. Synthesis, characterization, and applications of dendrimer-encapsulated nanoparticles. *The Journal of Physical Chemistry B*. 2005; 109(2): 692-704. Available from: https://doi.org/10.1021/jp0469665.
[25] Kong L, Alves CS, Hou W, Qiu J, Möhwald H, Tomás H, et al. RGD peptide-modified dendrimer-entrapped gold nanoparticles enable highly efficient and specific gene delivery to stem cells. *ACS Applied Materials & Interfaces*. 2015; 7(8): 4833-4843. Available from: https://doi.org/10.1021/am508760w.
[26] Yao G, Pei H, Li J, Zhao Y, Zhu D, Zhang Y, et al. Clicking DNA to gold nanoparticles: Poly-adenine-mediated formation of monovalent DNA-gold nanoparticle conjugates with nearly quantitative yield. *NPG Asia Materials*. 2015; 7: e159. Available from: https://doi.org/10.1038/am.2014.131.
[27] Drain CM, Varotto A, Radivojevi I. Self-organized porphyrinic materials. *Chemical Reviews*. 2009; 109(5): 1630-1658. Available from: https://doi.org/10.1021/cr8002483.
[28] Hu JS, Guo YG, Liang HP, Wan LJ, Jiang, L. Three-dimensional self-organization of supramolecular self-assembled porphyrin hollow hexagonal nanoprisms. *Journal of the American Chemical Society*. 2005; 127(48): 17090-17095. Available from: https://doi.org/10.1021/ja0553912.
[29] Jang JH, Jeon KS, Oh S, Kim HJ, Asahi T, Masuhara H, et al. Synthesis of Sn-porphyrin-intercalated trititanate nanofibers: Optoelectronic properties and photocatalytic activities. *Chemistry of Materials*. 2007; 19(8): 1984-1991. Available from: https://doi.org/10.1021/cm0629863.
[30] Jin CS, Lovell JF, Chen J, Zheng G. Ablation of hypoxic tumors with dose-equivalent photothermal, but not photodynamic, therapy using a nanostructured porphyrin assembly. *ACS Nano*. 2013; 7(3): 2541-2550. Available from: https://doi.org/10.1021/nn3058642.
[31] Li J, Zhu X, Wang JY, Rui ZY, Zhang SQ, Li YX, et al. Iron-containing porphyrins self-assembled on ZnO nanoparticles as electrocatalytic materials for oxygen reduction. *ACS Applied Nano Materials*. 2020; 3(1): 742-751. Available from: https://doi.org/10.1021/acsanm.9b02260.
[32] Liu L, Huang QW, Tanveer ZI, Jiang KQ, Zhang JH, Pan HY, et al. "Turn off-on" fluorescent sensor based on quantum dots and self-assembled porphyrin for rapid detection of ochratoxin A. *Sensors and Actuators B: Chemical*. 2020; 302: 8. Available from: https://doi.org/10.1016/j.snb.2019.127212.
[33] Lu XQ, Zhi FP, Shang H, Wang XY, Xue ZH. Investigation of the electrochemical behavior of multilayers film assembled porphyrin/gold nanoparticles on gold electrode. *Electrochimica Acta*. 2010; 55(11): 3634-3642. Available from: https://doi.org/10.1016/j.electacta.2009.11.004.
[34] Mandal S, Bhattacharyya S, Borovkov V, Patra A. Photophysical properties, self-assembly behavior, and energy transfer of porphyrin-based functional nanoparticles. *The Journal of Physical Chemistry C*. 2012; 116(20): 11401-11407. Available from: https://doi.org/10.1021/jp302462j.
[35] Ogawa K, Zhang TQ, Yoshihara K, Kobuke Y. Large third-order optical nonlinearity of self-assembled porphyrin oligomers. *Journal of the American Chemical Society*. 2002; 124(1): 22-23. Available from: https://doi.org/10.1021/ja0169015.
[36] Pan D, Liang PP, Zhong XM, Wang D, Cao H, Wang WJ, et al. Self-assembled porphyrin-based nanoparticles with enhanced near-infrared absorbance for fluorescence imaging and cancer photodynamic therapy. *ACS Applied Bio Materials*. 2019; 2(3): 999-1005. Available from: https://doi.org/10.1021/acsabm.8b00530.
[37] Wang L, Chen YL, Bian YZ, Jiang JZ. Porphyrin nanocrystal synthesized via chemical reaction route: ph-sensitive reversible transformation between nanocrystals and bulk single crystal. *The Journal of Physical Chemistry C*. 2013; 117(33): 17352-17359. Available from: https://doi.org/10.1021/jp4056544.
[38] Wang ZC, Medfort CJ, Shelnutt JA. Porphyrin nanotubes by ionic self-assembly. *Journal of the American Chemical Society*. 2004; 126(49): 15954-15955. Available from: https://doi.org/10.1021/ja045068j.
[39] Xiu Y, Xu LY, Zhang X, Wang X, Liu FY, Xia YQ, et al. Mechanistic process understanding of the biomimetic construction of porphyrin-based light-capturing antennas from self-assembled fmoc-blocked peptide templates. *ACS Sustainable Chemistry & Engineering*. 2020; 8(41): 15761-15771. Available from: https://doi.org/10.1021/

acssuschemeng.0c06191.
[40] Zhang N, Wang L, Wang, M, Cao RH, Wang JF, Bai F, et al. Self-assembled one-dimensional porphyrin nanostructures with enhanced photocatalytic hydrogen generation. *Nano Letters*. 2018; 18(1): 560-566. Available from: https://doi.org/10.1021/acs.nanolett.7b04701.
[41] Gao Y, Zhang X, Ma C, Li X, Jiang J. Morphology-controlled self-assembled nanostructures of 5,15-di[4-(5-acetylsulfanylpentyloxy)phenyl]porphyrin derivatives. Effect of metal−ligand coordination bonding on tuning the intermolecular interaction. *Journal of the American Chemical Society*. 2008; 130(50): 17044-17052. Available from: https://doi.org/10.1021/ja8067337.
[42] Cai WR, Zhang GY, Lu KK, Zeng HB, Cosnier S, Zhang XJ, et al. Enhanced electrochemiluminescence of one-dimensional self-assembled porphyrin hexagonal nanoprisms. *ACS Applied Materials & Interfaces*. 2017; 9(24): 20904-20912. Available from: https://doi.org/10.1021/acsami.7b05188.
[43] Ng KK, Lovell JF, Vedadi A, Hajian T, Zheng G. Self-assembled porphyrin nanodiscs with structure-dependent activation for phototherapy and photodiagnostic applications. *ACS Nano*. 2013; 7(4): 3484-3490. Available from: https://doi.org/10.1021/nn400418y.
[44] Yang J, An H-W, Wang H. Self-assembled peptide drug delivery systems. *ACS Applied Bio Materials*. 2021; 4(1): 24-46. Available from: https://doi.org/10.1021/acsabm.0c00707.
[45] Zhao LL, Xing YL, Wang R, Yu FF, Yu FB. Self-assembled nanomaterials for enhanced phototherapy of cancer. *ACS Applied Bio Materials*. 2020; 3(1): 86-106. Available from: https://doi.org/10.1021/acsabm.9b00843.
[46] Drain CM, Smeureanu G, Patel S, Gong X, Garno J, Arijeloye J. Porphyrin nanoparticles as supramolecular systems. *New Journal of Chemistry*. 2006; 30(12): 1834-1843. Available from: https://doi.org/10.1039/B607289E.
[47] Elashnikov R, Radocha M, Panov I, Rimpelova S, Ulbrich P, Michalcova A, et al. Porphyrin-silver nanoparticles hybrids: Synthesis, characterization and antibacterial activity. *Materials Science and Engineering: C*. 2019; 102: 192-199. Available from: https://doi.org/10.1016/j.msec.2019.04.029.
[48] Gong XC, Milic T, Xu C, Batteas JD, Drain CM. Preparation and characterization of porphyrin nanoparticles. *Journal of the American Chemical Society*. 2002; 124(48): 14290-14291. Available from: https://doi.org/10.1021/ja027405z.
[49] Bera R, Mandal S, Mondal B, Jana B, Nayak SK, Patra A. Graphene–porphyrin nanorod composites for solar light harvesting. *ACS Sustainable Chemistry & Engineering*. 2016; 4(3): 1562-1568. Available from: https://doi.org/10.1021/acssuschemeng.5b01504.
[50] Kang S, Yasuda M, Miyasaka H, Hayashi H, Kawasaki M, Umeyama T, et al. Light harvesting and energy transfer in multiporphyrin-modified CdSe nanoparticles. *ChemSusChem*. 2008; 1(3): 254-261. Available from: https://doi.org/10.1002/cssc.200700138.
[51] Chen Y, Li A, Huang Z-H, Wang L-N, Kang F. Porphyrin-based nanostructures for photocatalytic applications. *Nanomaterials*. 2016; 6(3): 51. Available from: https://doi.org/10.3390/nano6030051.
[52] Ussia M, Bruno E, Spina E, Vitalini D, Pellegrino G, Ruffino F, et al. Freestanding photocatalytic materials based on 3D graphene and polyporphyrins. *Scientific Reports*. 2018; 8: 5001. Available from: https://doi.org/10.1038/s41598-018-23345-y.
[53] Gawande MB, Goswami A, Asefa T, Guo HZ, Biradar AV, Peng DL, et al. Core-shell nanoparticles: Synthesis and applications in catalysis and electrocatalysis. *Chemical Society Reviews*. 2015; 44(21): 7540-7590. Available from: https://doi.org/10.1039/c5cs00343a.
[54] Mandal S, Bhattacharyya S, Borovkov V, Patra A. Porphyrin-based functional nanoparticles: conformational and photophysical properties of bis-porphyrin and bis-porphyrin encapsulated polymer nanoparticles. *The Journal of Physical Chemistry C*. 2011; 115(49): 24029-24036. Available from: https://doi.org/10.1021/jp208819b.
[55] Rotomskis R, Augulis R, Snitka V, Valiokas R, Liedberg B. Hierarchical structure of TPPS4 J-aggregates on substrate revealed by atomic force microscopy. *The Journal of Physical Chemistry B*. 2004; 108(9): 2833-2838. Available from: https://doi.org/10.1021/jp036128v.
[56] Filippini D, Alimelli A, Di Natale C, Paolesse R, D'Amico A, Lundström I. Chemical sensing with familiar devices. *Angewandte Chemie International Edition*. 2006; 45(23): 3800-3803. Available from: https://doi.org/10.1002/anie.200600050.
[57] Malinski T, Taha Z. Nitric oxide release from a single cell measured in situ by a porphyrinic-based microsensor. *Nature*. 1992; 358(6388): 676-678. Available from: https://doi.org/10.1038/358676a0.
[58] Lo P-C, Huang J-D, Cheng DYY, Chan EYM, Fong W-P, Ko W-H, et al. New amphiphilic silicon(IV) phthalocyanines as efficient photosensitizers for photodynamic therapy: Synthesis, photophysical properties, and in vitro photodynamic activities. *Chemistry – A European Journal*. 2004; 10(19): 4831-4838. Available from: https://doi.org/10.1002/chem.200400462.

[59] Paul AK, Jayaram DT, Babu PSS, Adarsh N, Thurakkal S, Nair AS, et al. Synthesis and *in vitro* photobiological studies of porphyrin capped gold nanoparticles[§]. *Journal of Chemical Sciences.* 2018; 130(10): 133. Available from: https://doi.org/10.1007/s12039-018-1539-8.
[60] Wang J, Zhong Y, Wang L, Zhang N, Cao R, Bian K, et al. Morphology-controlled synthesis and metalation of porphyrin nanoparticles with enhanced photocatalytic performance. *Nano Letters*. 2016; 16(10): 6523-6528. Available from: https://doi.org/10.1021/acs.nanolett.6b03135.
[61] Wang JF, Zhong Y, Wang X, Yang WT, Bai F, Zhang BB, et al. pH-dependent assembly of porphyrin-silica nanocomposites and their application in targeted photodynamic therapy. *Nano Letters*. 2017; 17(11): 6916-6921. Available from: https://doi.org/10.1021/acs.nanolett.7b03310.
[62] Chaudhuri G, Paria S. Core/shell nanoparticles: classes, properties, synthesis mechanisms, characterization, and applications. *Chemical Reviews*. 2012; 112(4): 2373-2433. Available from: https://doi.org/10.1021/cr100449n.
[63] Lee J, Lee Y, Youn JK, Na HB, Yu T, Kim H, et al. Simple synthesis of functionalized superparamagnetic magnetite/silica core/shell nanoparticles and their application as magnetically separable high-performance biocatalysts. *Small*. 2008; 4(1): 143-152. Available from: https://doi.org/10.1002/smll.200700456.
[64] Filho MAM, Hsiao C-L, dos Santos RB, Hultman L, Birch J, Gueorguiev GK. Self-induced core-shell InAlN nanorods: Formation and stability unraveled by ab initio simulations. *ACS Nanoscience Au*. 2023; 3(1): 84-93. Available from: https://doi.org/10.1021/acsnanoscienceau.2c00041.
[65] Lundgren C, Kakanakova-Georgieva A. Gueorguiev GKA perspective on thermal stability and mechanical properties of 2D Indium Bismide from *ab initio* molecular dynamics. *Nanotechnology*. 2022; 33(33). Available from: https://doi.org/10.1088/1361-6528/ac6baf.
[66] Sangiovanni DG, Faccio R, Gueorguiev GK, Kakanakova-Georgieva A. Discovering atomistic pathways for supply of metal atoms from methyl-based precursors to graphene surface. *Physical Chemistry Chemical Physics*. 2022; 25(1): 829-837. Available from: https://doi.org/10.1039/d2cp04091c.
[67] Kanaizuka K, Izumi A, Ishizaki M, Kon H, Togashi T, Miyake R, et al. Molecular nanostamp based on one-dimensional porphyrin polymers. *ACS Applied Materials & Interfaces*. 2013; 5(15): 6879-6885. Available from: https://doi.org/10.1021/am401123r.
[68] Kawaguchi T, Okamura S, Togashi T, Harada W, Hirahara M, Miyake R, et al. Potential tuning of nanoarchitectures based on phthalocyanine nanopillars: Construction of effective photocurrent generation systems. *ACS Applied Materials & Interfaces*. 2015; 7(34): 19098-19103. Available from: https://doi.org/10.1021/acsami.5b04646.
[69] Togashi T, Izumi A, Kon H, Kanaizuka K, Ishizaki M, Miyake R, et al. Spontaneous construction of nanoneedles using ruthenium complex-conjugated porphyrins on substrates. *Chemistry Letters*. 2014; 43(8): 1201-1203. Available from: https://doi.org/10.1246/cl.140256.
[70] Chambers PC, Kuruppu Arachchige NMK, Taylor AM, Garno JC. Surface coupling of octaethylporphyrin with silicon tetrachloride. *ACS Omega*. 2019; 4(2): 2565-2576. Available from: https://doi.org/10.1021/acsomega.8b03204.
[71] Kucheryavy P, He J, John VT, Maharjan P, Spinu L, Goloverda GZ, et al. Superparamagnetic iron oxide nanoparticles with variable size and an iron oxidation state as prospective imaging agents. *Langmuir*. 2013; 29: 710-716. Available from: https://doi.org/10.1021/la3037007.
[72] Komati R, Mitchell CA, LeBeaud A, Do H, Goloverda GZ, Kolesnichenko VL. Tenacic acids: A new class of tenacious binders to metal oxide surfaces. *Chemistry – A European Journal*. 2018; 24(55): 14824-14829. Available from: https://doi.org/10.1002/chem.201803242.
[73] Grabar KC, Freeman RG, Hommer MB, Natan MJ. Preparation and characterization of Au colloid monolayers. *Analytical Chemistry*. 2002; 67(4): 735-743. Available from: https://doi.org/10.1021/ac00100a008.
[74] Nečas D, Klapetek P. Gwyddion: An open-source software for SPM data analysis. *Central European Journal of Physics*. 2012; 10(1): 181-188. Available from: https://doi.org/10.2478/s11534-011-0096-2.
[75] Lee DC, Morales GM, Lee Y, Yu L. Cofacial porphyrin multilayers via layer-by-layer assembly. *Chemical Communications*. 2006; 100-102. Available from: https://doi.org/10.1039/b512084e.
[76] Giovannetti, R The use of spectrophotometry UV-Vis for the study of porphyrins. In: Uddin J. (ed.) *Macro to nano spectroscopy*. Rijeka, Croatia: Intech; 2012. p.87-108. Available from: https://doi.org/10.5772/38797.